Theory of the light-force technique for measuring polarizabilities

Keith D. Bonin and Michael A. Kadar-Kallen
Department of Physics, Wake Forest University, Winston-Salem, North Carolina 27109-7507
(Received 22 June 1992)

The theory of a method to measure electric-dipole polarizabilities is presented. The method uses two-stage laser ablation to produce a pulsed beam of atoms from a solid target. A pair of slits makes the velocity distribution of the atomic beam nonuniform in a way that is well characterized. The light-force technique uses the polarization forces experienced by an atom in the intense, inhomogeneous electromagnetic field of a standing-wave laser to change the velocity distribution of the atomic beam. The large forces cause measurable Doppler shifts in the resonant frequency of the atoms. These frequency shifts change the amount of absorption of resonant light, yielding information about the change in the velocity distribution of the atoms. The detailed shape of the final absorption distribution is polarizability dependent. In the classical picture of the light force, the standing-wave *electric* field induces a time-varying dipole moment in each atom. Each atom then experiences a Lorentz force due to coherent interaction of the oscillating dipole moment with the time-varying *magnetic* field. The quantum-mechanical picture corresponds to the Kapitza-Dirac effect for atoms: an atom absorbs a photon from one of the two beams which form the standing wave, and is then stimulated to emit this photon by the other, counterpropagating beam. This paper provides a classical treatment of the light force experienced by an atom in a standing-wave light field; the polarizability is treated quantum mechanically. The theory presented here can be applied to atoms with a scalar polarizability, such as rubidium, and to atoms with significant tensor components, such as uranium. Experimental results from application of the light-force technique to a measurement of the polarizability of rubidium are also presented.

PACS number(s): 35.10.Di, 42.50.Vk, 35.80 + s

I. INTRODUCTION

The polarizability is a measure of the size of the charge separation that results when an atom or molecule is placed in an electric field. If an atom is placed in a static electric field $\mathbf{E}$, the nucleus will be displaced from the center of charge of the electrons, and the atom will acquire an electric-dipole moment $\mathbf{p}$. If the field is not too large, and the response of the atom is isotropic, the induced dipole moment will be proportional to the electric field, and one can write

$$\mathbf{p} = \alpha \mathbf{E}. \tag{1}$$

The constant of proportionality α is called the polarizability of the atom. The polarizability is a fundamental property of atoms that characterizes the lowest-order response of an atom to an applied electric field. In cgs units, the polarizability has the units of volume and is of the same order of magnitude as the volume of the atom ($\approx 10^{-23}$ cm^3).

The polarizability determines the values of many important physical properties of atoms and molecules such as ion-atom charge-exchange cross sections, van der Waals constants, ion mobilities in gases, and refractive indices (dielectric constants). A number of methods have been developed for measuring polarizabilities including beam deflection [1], refractive index [2], the E-H gradient balance technique [3], and others [4]. However, for most elements in the Periodic Table (75%), the electric-dipole polarizability remains unmeasured. The strengths and limitations of the traditional methods mentioned above have been discussed in the excellent review articles by Miller and Bederson [5, 6]. It is particularly difficult to measure the polarizability of refractory-metal atoms due to the difficulty of producing beams and due to the complexity in making a gas cell of uniform density. Detection of most refractory-metal atoms is also a significant problem [6]. This paper discusses a method called the light-force technique, which is specifically designed to address the problems of determining polarizabilities of refractory-metal atoms. It has been used to measure the polarizability of rubidium [7] and experiments are currently underway to determine the polarizability of an important refractory-metal element: uranium. The theory presented here can be applied to an atom with a scalar polarizability, for example, rubidium, and to atoms that have significant tensor components, such as uranium.

Presently, we briefly describe the light-force technique. For now consider the simple picture of an atom with a scalar polarizability α located in a *static* electric field $\mathbf{E}$. If the electric field is a function of position, then an atom will experience a conservative force that is the negative gradient of a potential energy

$$U = -\frac{1}{2}\alpha E^2. \tag{2}$$

The conservative force $\mathbf{F}_c$ is given by

$$\mathbf{F}_c = -\nabla U = \alpha E \nabla E. \tag{3}$$

Thus atoms in regions with large fields and large field

gradients experience large forces. In the light-force technique a beam of atoms is sent through a standing wave formed by an intense, pulsed Nd:YAG laser (where YAG denotes yttrium aluminum garnet). Forming a standing wave with the light from a low-frequency laser produces stationary (cycle-averaged) potentials that vary spatially from zero to a maximum value over regions the size of a half-wavelength of light. Atoms traversing an intense standing-wave field will experience a range of forces from zero to very large (accelerations $> 10^8$ g's where g is the acceleration due to gravity at the surface of the Earth), depending on their position in the field. The experimental sketch given in Fig. 1 reflects this physical situation. Here, two of the three atoms traverse regions of large $E\nabla E$ and receive significant deflections. The other atom shown traverses an antinode of the standing-wave field and is not deflected. Deflected atoms have their resonant frequencies Doppler shifted with respect to undeflected atoms. The light force is detected by observing the change in absorption of light tuned near resonance. Deflected atoms are Doppler detuned from the frequency of light provided by a probe laser that intersects the atomic beam downstream from the light-force region. As a result of these Doppler detunings, the transmitted light is increased — see Fig. 1. A measurement of the change in transmitted light and a measurement of the unidirectional fluence (energy per area) of the standing-wave laser provide enough information to determine a value of the polarizability of the atoms traversing the standing wave.

The technique has a number of salient features:

(i) The technique takes advantage of the large fields that modern pulsed lasers are capable of producing.

(ii) The field gradients are large because the field varies over distances of a wavelength of light.

(iii) The atomic beam is pulsed, a natural match to the pulsed light-force laser. Laser ablation produced a pulsed beam with an atomic density larger than that achievable with traditional beam sources. Pulsing the atomic beam reduces the amount of material consumed and it obviates the need for the large pumps required for supersonic nozzle beams.

(iv) The technique relies on an accurate measurement of the laser fluence and of the absorption of a probe laser beam as a function of the mean atom velocity. The light-force technique provides an *absolute* measurement of the polarizability. It does *not* rely on a relative measurement which is referenced to a calibration atom.

(v) The technique could be used to measure radicals and other short-lived species.

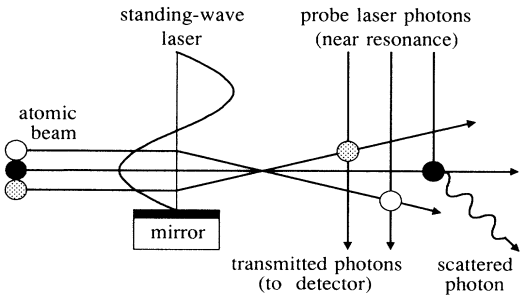

FIG. 1. The change in the velocity distribution due to the standing-wave laser may be measured by observing the absorption of resonant light just downstream of the standing-wave region. Atoms that receive significant velocity kicks are Doppler detuned from resonance and scatter fewer photons. Atoms that experience no net force remain tuned on resonance and continue to scatter photons at a high rate.

The theory presented here treats the atomic polarizabilities quantum mechanically, while the light force is treated classically. The quantum picture of the light force is that of the off-resonant Kapitza-Dirac effect. The standing-wave light field is composed of propagating and counterpropagating light beams. An atom in such a field can absorb a photon from one beam and be stimulated to emit a photon by the other beam. This results in momentum changes to the atom that are integer multiples of $2\hbar\mathbf{k}$, where $\mathbf{k}$ is the wave vector of a photon in the beam. Since the quantized nature of the stimulated scattering is not observed in these experiments and a classical treatment is adequate to explain our results, a fully quantum treatment is not presented here. A quantum treatment for the *near-resonant* case has been given to explain observations that did resolve the quantized nature of the stimulated scattering in the Kapitza-Dirac effect for atoms [8].

Our approach is straightforward: we first present a theoretical description of the light force and discuss its effect on the distribution of atoms in phase space. The next section quantitatively describes detection of the effects of the light force. We then give a detailed description of the application of the technique to rubidium. The final section provides a summary and conclusions. In each section, we have taken care to discuss limitations of the technique, both from a physical standpoint and from a technical standpoint.

II. THEORY OF THE LIGHT FORCE

A. The light force

To understand the light-force technique, it is useful to study the equations of motion for atoms that traverse a given region of the standing-wave field. The force on an atom is due to the ac fields acting on the induced dipole, since ac fields will have, on average, no effect on a permanent electric or magnetic dipole. To sketch a derivation of the force, consider an atom located in the harmonic electric field

$$\mathbf{E}(\mathbf{x},t)=\frac{1}{2}\left[\mathbf{E}_0(\mathbf{x})e^{-i\omega t}+\text{c.c.}\right], \tag{4}$$

where ω is the angular frequency of the oscillating field and c.c. refers to the complex conjugate. If the atom has been in the field for a sufficiently long time it will acquire a steady-state dipole moment that is also harmonic in time and follows the field:

$$\mathbf{p}(\mathbf{x},t)=\frac{1}{2}\left[\mathbf{p}_0(\mathbf{x})e^{-i\omega t}+\text{c.c.}\right], \tag{5}$$

where the amplitude $\mathbf{p}_0(\mathbf{x})$ of the oscillating dipole moment is proportional to the amplitude $\mathbf{E}_0(\mathbf{x})$ of the oscillating field.

If the atomic electrons have a net angular momentum $J > 1/2$ in the ground state of the atom, the induced dipole moment will depend on the spin polarization of the atoms and can be anisotropic. That is, the polarization of the atom will be proportional to the external field, but the direction of the induced dipole moment may not be the same as the direction of the applied field. We must then describe the dipole moment induced in the atom with a polarizability tensor α_{ij} where the indices label the axes of a Cartesian coordinate system. The ith component of the amplitude of the oscillating electric dipole moment is

$$p_{0i}(\mathbf{x}) = \sum_j \alpha_{ij} E_{0j}(\mathbf{x}), \tag{6}$$

or equivalently

$$\mathbf{p}_0(\mathbf{x}) = \boldsymbol{\alpha} \cdot \mathbf{E}_0(\mathbf{x}). \tag{7}$$

Both the dipole moment and the polarizability should be thought of as expectation values, which depend on the spin polarization of the atoms in their ground state. For example, $\alpha_{ij} = \mathrm{Tr}\,(\rho\,\hat{\alpha}_{ij})$, where ρ is the density matrix of the polarized atoms, $\hat{\alpha}_{ij}$ is the polarizability tensor operator, and the trace operation extends over all spin sublevels of the atom. However, for the light-force technique it is useful to consider the diagonal matrix elements of the polarizability tensor operator $\langle m|\hat{\alpha}_{ij}|m\rangle = \alpha_{ij}(m)$, where m is an eigenvalue of the operator J_z, which is the projection of the angular momentum on the axis of quantization.

The frequency-dependent polarizability tensor $\boldsymbol{\alpha}(\omega) = \boldsymbol{\alpha}'(\omega) + i\boldsymbol{\alpha}''(\omega)$ is the sum of a Hermitian part $\boldsymbol{\alpha}'(\omega)$ and an anti-Hermitian part $i\boldsymbol{\alpha}''(\omega)$. The anti-Hermitian part of the polarizability tensor accounts for the dissipation of the incident field by the absorption of light. It reaches maximum values at atomic resonances (where $\boldsymbol{\alpha}'$ is zero). When the frequency of the field is far from all resonances the anti-Hermitian part of the polarizability is negligible ($\boldsymbol{\alpha}'' \ll \boldsymbol{\alpha}'$). This is the case for the theory and experiments presented here. Henceforth, we shall only consider the Hermitian part of the polarizability and for convenience we shall presume $\boldsymbol{\alpha} \equiv \boldsymbol{\alpha}'$. The polarizability tensor is discussed more extensively in the Appendix.

An atom in an oscillating field that is far from any atomic resonances experiences a time-averaged force that is conservative. This conservative dipole force is the negative gradient of a time-averaged potential and is given by

$$\langle \mathbf{F} \rangle = -\boldsymbol{\nabla}\langle \mathrm{U} \rangle = -\boldsymbol{\nabla}\left(\frac{1}{4}\mathbf{E}_0^* \cdot \boldsymbol{\alpha} \cdot \mathbf{E}_0\right), \tag{8}$$

where the angular brackets imply a time average over an optical cycle. The above result can be derived from the Lorentz force on an atom at position $\mathbf{x}$.

In an oscillating field the total force on an atom to lowest order in d/λ, where d is the "diameter" of an atom and λ is the wavelength of light, is given by

$$\mathbf{F}(\mathbf{x},t) = \mathbf{p}(\mathbf{x},t) \cdot \boldsymbol{\nabla}\mathbf{E}(\mathbf{x},t) + \frac{1}{c}\frac{\partial \mathbf{p}(\mathbf{x},t)}{\partial t} \times \mathbf{B}(\mathbf{x},t), \tag{9}$$

where c is the speed of light and $\mathbf{B}(\mathbf{x},t)$ is the magnetic field at position $\mathbf{x}$ and at time t. The first term in Eq. (9) is the force on an electric dipole in an electric-field gradient. It is the lowest-order nonvanishing force on an atom in a nonuniform *static* electric field. The second term represents the magnetic force on the moving charges inside the atom. In a plane traveling-wave or plane standing-wave field the first term is zero; only the second term contributes to the force. The time-varying force on an atom in an electromagnetic standing wave is illustrated in Fig. 2.

For completeness, we mention that the light force manifests itself as the negative gradient of the expectation value of the light-shift operator. The light-shift operator $\delta\hat{\mathcal{E}}$ corresponds to the Hermitian part of the light-atom interaction Hamiltonian and is given by [9]

$$\delta\hat{\mathcal{E}} = -\frac{|E_0|^2}{8}(\hat{\boldsymbol{\epsilon}}^* \cdot \hat{\boldsymbol{\alpha}} \cdot \hat{\boldsymbol{\epsilon}} + \hat{\boldsymbol{\epsilon}} \cdot \hat{\boldsymbol{\alpha}}^\dagger \cdot \hat{\boldsymbol{\epsilon}}^*), \tag{10}$$

where $\hat{\boldsymbol{\epsilon}}$ is the polarization vector of the applied electric field and the $\hat{\boldsymbol{\alpha}}$'s are operators. The light-shift operator and observations of its behavior in optically-pumped systems have been extensively discussed elsewhere [9, 10]. A major difference between our experiments and investigations of others that also utilized the light-shift operator is that we use standing waves, not traveling waves. This produces significant and predictable small-scale spatial structure on the operator. The presence of this spatial

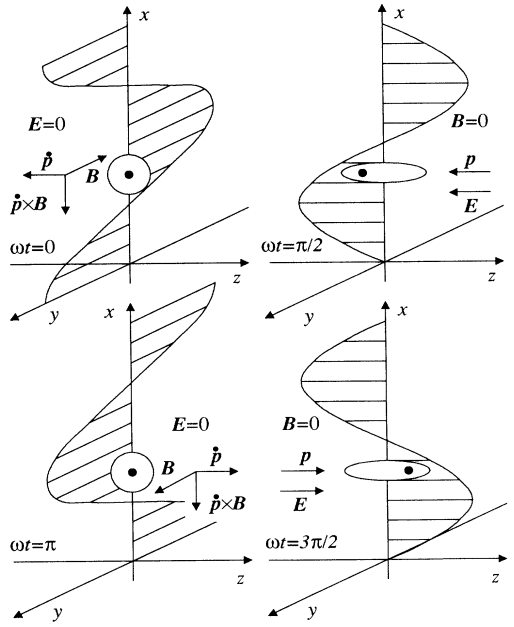

FIG. 2. An atom in an electromagnetic standing wave, at four instants of time. For illustration: the atom has a real scalar polarizability; the incident plane wave has an electric field $\mathbf{E}=\mathcal{E}_0\hat{\mathbf{z}}\cos(-kx-\omega t)$; and the mirror is the plane $x=0$ with a complex reflectivity of -1. The standing-wave field is then $\mathbf{E}=-2\mathcal{E}_0\hat{\mathbf{z}}\sin kx\sin\omega t$, $\mathbf{B}=2\mathcal{E}_0\hat{\mathbf{y}}\cos kx\cos\omega t$. It follows that $\mathbf{p}\cdot\nabla\mathbf{E}\equiv 0$ so that the force on the atom is due entirely to the term $(1/c)\dot{\mathbf{p}}\times\mathbf{B}$ in Eq. (9).

structure is the key to the light-force technique.

For simplicity, consider a standing-wave field produced by retroreflecting a uniform, monochromatic plane wave using a mirror at $x = 0$ that causes no change in the phase of the electric field upon reflection and has a reflectivity of -1. Assume the wave is linearly polarized along $\hat{z}$ and propagating in the $-\hat{\mathbf{x}}$ direction. The electric-field amplitude of the incident plane wave is

$$\mathbf{E}_0^{(i)} = \mathcal{E}_0 \hat{\mathbf{z}} \exp(-ikx), \tag{11}$$

where $\mathcal{E}_0$ is real. The laser is reflected in the $+\hat{\mathbf{x}}$ direction with a field amplitude of

$$\mathbf{E}_0^{(r)} = -\mathcal{E}_0 \hat{\mathbf{z}} \exp(ikx), \tag{12}$$

so that the total electric field above the mirror is

$$\mathbf{E}_0 = -2i\mathcal{E}_0 \hat{\mathbf{z}} \sin(kx). \tag{13}$$

The time-averaged polarization potential is therefore [see Eq. (8)]

$$\langle \mathrm{U} \rangle = \mathcal{E}_0^2 \alpha_{zz} \sin^2(kx), \tag{14}$$

with a resulting force of

$$\langle \mathbf{F} \rangle = k\mathcal{E}_0^2 \alpha_{zz} \sin(2kx)\hat{\mathbf{x}}. \tag{15}$$

The force on the atom depends linearly on α_{zz}, the component of the polarizability tensor selected by the polarization of the incident laser. The force is along $\hat{\mathbf{x}}$, normal to the surface of the mirror, and is periodic in x with a spatial frequency of $2k$. Hence the spatial period of the force is $\Lambda = \lambda/2$. The magnitude of the force is proportional to the wave number k of the standing wave and to its intensity $c\mathcal{E}_0^2/(8\pi)$.

In a real experiment these results must be modified to incorporate the temporal and spatial structure that is present on the laser beam. Since the laser beam has spatial structure, the force on an atom will depend on its location within the beam. The force on an atom will also vary in time since the laser beam is pulsed. A more realistic expression for the applied incident electric field is

$$\mathbf{E}(\mathbf{x}, t) = \mathrm{Re}\left[\left(\frac{8\pi \mathcal{F}(y,z) f(t)}{c}\right)^{1/2} \hat{\boldsymbol{\varepsilon}} \exp(-ikx - i\omega t)\right], \tag{16}$$

where

$$\mathcal{F}(y,z) = \frac{c}{8\pi} \int_{-\infty}^{\infty} \mathbf{E}^2(\mathbf{x}, t) dt \tag{17}$$

is the fluence (energy per area) of the laser pulse and $\hat{\boldsymbol{\varepsilon}}$ is the polarization vector of the incident electric field [11]. The quantity $f(t)$ is the slowly varying, time-dependent envelope of the laser pulse. The envelope function is chosen to be normalized over a single pulse so that

$$\int_{-\infty}^{\infty} f(t) dt = 1. \tag{18}$$

The time-averaged force Eq. (8) now becomes

$$\langle \mathbf{F} \rangle = \frac{8\pi}{c} k \mathcal{F}(y,z) f(t) \, (\hat{\boldsymbol{\varepsilon}}^* \cdot \boldsymbol{\alpha} \cdot \hat{\boldsymbol{\varepsilon}}) \sin(2kx)\hat{\mathbf{x}}. \tag{19}$$

The force only affects the motion along one dimension (along $\hat{\mathbf{x}}$). The equation of motion for an atom can be written

$$\frac{d^2x}{dt^2} = V(y,z) f(t) \sin(2kx), \tag{20}$$

where the characteristic velocity V is

$$V(y,z) = \frac{16\pi^2}{M\lambda_{\mathrm{sw}} c} \mathcal{F}(y,z) \, (\hat{\boldsymbol{\varepsilon}}^* \cdot \boldsymbol{\alpha} \cdot \hat{\boldsymbol{\varepsilon}}), \tag{21}$$

where λ_{sw} is the wavelength of the standing wave laser and M is the mass of the atom. Physically, the characteristic velocity corresponds to the maximum kick that can be given to an atom by the light force. Since we have no need to refer to the (total) atomic velocity, we use the term "velocity" to refer to the x component of the velocity of the atom, and label v_x as v. The motion in x of an atom affected by the light force can be expressed by the pair of first-order differential equations

$$\begin{aligned} \frac{dx}{dt} &= v, \\ \frac{dv}{dt} &= V(y,z) f(t) \sin(2kx). \end{aligned} \tag{22}$$

It is important to note that if the total angular momentum of the atoms is such that $J > 1/2$, then the atoms will experience different forces depending on their magnetic sublevel, even if the electric field and field gradient at the location of each atom is identical. The Stern-Gerlach experiment serves as a good analogy to the light-force experiment in the case of an atomic species with a tensor polarizability ($J > 1/2$) — see Fig. 3. For simplicity, consider the case where each atom traverses a region with a given electric field and electric-field gradient. The electric field is assumed to be linearly polarized along the quantization axis, i.e., $\hat{\boldsymbol{\varepsilon}} = \hat{\mathbf{z}}$. It is then clear from Eqs. (20) and (21) that the characteristic velocity of an atom, and hence the force on an atom, will depend on the α_{zz} component of the polarizability tensor. From the Appendix, this component of the polarizability tensor depends on the magnetic sublevel of the atom—see Eq. (A9). Thus atoms in different magnetic sublevels will experience different forces, resulting in space and velocity separation of the atomic beam as in the classic Stern-Gerlach experiment. The similarities and differences between the Stern-Gerlach experiment and the light-force experiment are illustrated in Fig. 3 for the case of an atom with $J = 3/2$. The major difference between the two experiments is that the light force is usually independent of the *sign* of the magnetic sublevel quantum number m. Another difference is that the distinct separation of the $|m|$ sublevels is washed out in the light-force experiments because the atomic beam samples several hundred spatial periods of the standing wave. Hence the

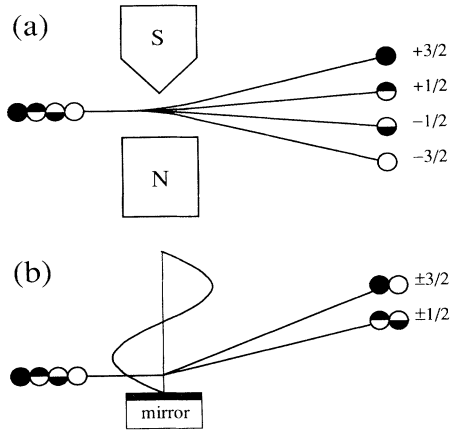

FIG. 3. (a) In the Stern-Gerlach experiment, an inhomogeneous magnetic field provides the force that splits an atomic beam into $2J+1$ beams. (b) In the light-force experiment, an inhomogeneous electromagnetic field produced by a standing wave of light provides the force that splits an atomic beam into $J+1/2$ beams for half-integral J, or into $J+1$ beams for integral J.

atomic beam samples a continuous distribution of electric fields and electric-field gradients, resulting in a continuous distribution of final velocity and position states. The light force will only depend on the *sign* of m (the vector part of the polarizability tensor—see the Appendix) in the case of circularly polarized light *and* for frequencies that are not small compared to atomic frequencies. Hereafter, any contribution from the vector part of the polarizability tensor is neglected.

In general, the light-shift operator shifts the energy of each magnetic sublevel. However, the light-shift operator can also cause transitions between sublevels. Such transitions will only occur when the population distribution among the ground-state magnetic sublevels is anisotropic. Here the density matrix evolves according to

$$\rho(t) = \exp\left(-\frac{i}{\hbar}\int_{t_0}^{t}\delta\hat{\mathcal{E}}dt'\right)\rho(t_0)\left(\frac{i}{\hbar}\int_{t_0}^{t}\delta\hat{\mathcal{E}}dt'\right), \qquad (23)$$

where the light-shift operator $\delta\hat{\mathcal{E}}$ is given by Eq. (10). The general case of arbitrary population distribution and light polarization is quite complicated and we do not consider it further here. Instead we consider the case where the initial atomic population has a statistical distribution among the magnetic sublevels with

$$\langle Jm|\rho(t_0)|Jm\rangle = \frac{1}{2J+1} \quad \forall\, m. \qquad (24)$$

Then the populations of the different sublevels will remain unchanged, regardless of the polarization properties of the light. This choice is also practical since it matches our experimental conditions.

B. Limitations to the light force

It is important to discuss factors that limit the magnitude of the force in the light-force technique. The size of the light force depends linearly on the magnitude of the electric field $\mathcal{E}_0$ and on its gradient $\mathcal{E}_0/\lambda$. Therefore, best results would occur for maximum values of these quantities. Both of these quantities increase with increasing laser fluence. However, physical processes such as linear excitation, nonlinear excitation, and ionization will eventually dominate at high enough fluences. These processes depend on the laser wavelength as well. Although shorter wavelengths produce larger field gradients, the wavelength must remain far enough away from resonances that the conservative part of the light interaction dominates the dissipative part. Additionally, the coherence length of the light-force laser is important in achieving high field gradients. The visibility of the light fringes is directly determined by the coherence length. The coherence length must at least be on the order of a centimeter to ensure that the interaction region of the laser and atoms is well away from the retroreflecting mirror. This limits the temporal pulse width τ of the light-force laser to a few picoseconds (or longer). Also, the temporal pulse width cannot be so long that individual atoms given velocity kicks by the force have time to sample several standing-wave fringes. This would essentially average out to a net force of zero. This physical condition can be expressed quantitatively as

$$V\tau \ll \Lambda. \qquad (25)$$

The maximum size of the force is also limited for technical reasons. For example, the retroreflecting standing-wave mirror has a damage threshold that limits the maximum fluence that can be applied to the atoms. The best dielectric mirrors cannot withstand intensities in excess of $5-10$ GW/cm^2.

C. The Liouville theorem and atomic phase space

To detect a measurable effect due to the light force, the atoms must be prepared in a nonuniform distribution in phase space since the force is conservative. From Liouville's theorem, the density of particles in phase space cannot change in a conservative system, and hence a uniform distribution of particles will remain so under the action of a conservative potential [12]. Atoms are prepared in a nonuniform distribution by phase-space filtering the atomic beam with a pair of slits (see Fig. 4). After passing through a pair of slits, the atoms traverse the standing-wave region, where the polarization force redistributes the atoms in phase space. The effects of the force can be detected by measuring the redistribution of atoms in *configuration space* and/or by measuring the redistribution of atoms in *velocity space*. We measure the redistribution in velocity space by measuring the change in absorption of resonant light that occurs due to the Doppler shift that results when an atom is given a momentum kick by the light force — see Fig. 1.

In evaluating the density of points in the phase space

(x, v) we follow the trajectory of atoms which start at some position (y, z) and have y and z velocities v_y and v_z [13]. For example, the phase-space distribution produced by a pair of matched slits, each having width w, is shown in Fig. 4. Figure 5 illustrates the redistribution of atoms in phase space due to application of the light force from a standing-wave laser located just downstream of the second slit. These plots, which show the evolution of the phase-space distribution over time during a laser pulse, were generated by numerically integrating the equations of motion Eq. (22). The time dependence of the laser was chosen to be Gaussian, a good approximation in these experiments:

$$f(t) = \frac{1}{\tau\sqrt{2\pi}} \exp\left[-\frac{1}{2}\left(\frac{t}{\tau}\right)^2\right]. \tag{26}$$

Here $2\tau\sqrt{2\ln 2}$ is the full width at half maximum (FWHM) of the standing-wave-laser pulse.

In these experiments, we are interested in the x-velocity distribution of the atoms, characterized by the velocity probability density $p(v)$, where $p(v)dv$ is the probability of finding an atom in the velocity range between v and $v + dv$. To find the final probability density $p(v_f)$ of the atoms after the standing-wave pulse, the equations of motion Eq. (22) must be solved.

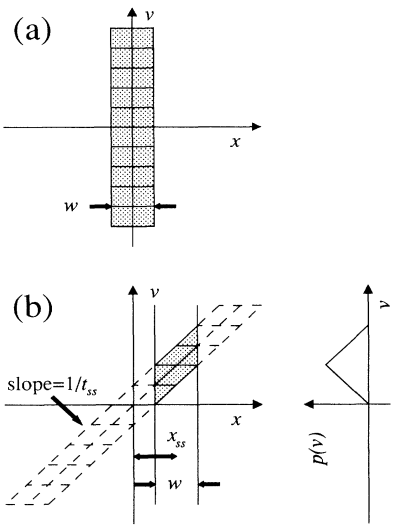

FIG. 4. The phase-space distribution in (x, v) due to a pair of slits of equal width which limit the motion of an atom in x. We follow only those atoms which at time $t = 0$ are located at $z = z_0$ and which have a z velocity v_z. The distribution in (x, v) is assumed to be independent of y and v_y. (a) The atoms reach the first slit at $t = (z_{s1} - z_0)/v_z$ (where $z = z_{s1}$ is the first slit plane). The distribution of atoms in (x, v) is assumed to be uniform before the atoms reach the first slit which passes only those atoms in the region $\{x : |x| < w/2\}$. (b) The atoms encounter the second slit after an additional time $t_{ss} = z_{ss}/v_z$ has elapsed (where z_{ss} is the longitudinal separation of the slits). Only those atoms in the region $\{x : |x - x_{ss}| < w/2\}$ are allowed to pass. The resulting velocity distribution is triangular.

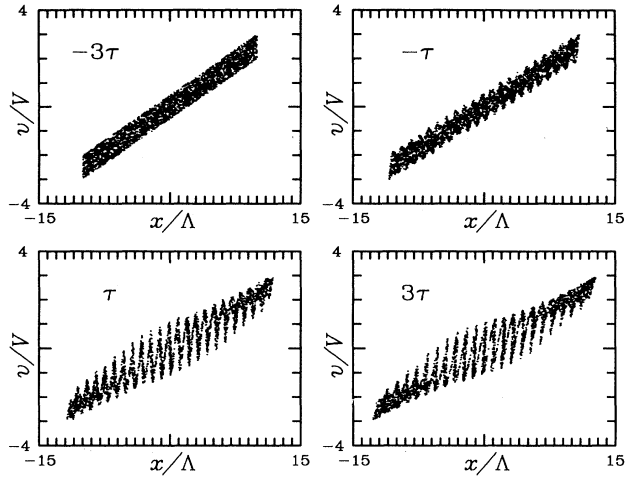

FIG. 5. Evolution of the distribution of atoms in (x, v) under the action of a standing-wave laser. The four instants of time shown are equally spaced from $t - t_{sw} = -3\tau$ to $t - t_{sw} = +3\tau$ for a Gaussian shaped laser pulse [see Eq. (26)]. The initial distribution is that formed by a pair of slits which limit the motion of atoms in x. For illustration, the first slit has been chosen to be much narrower than the second and $V\tau = \Lambda/(2\pi)$. The final distribution in phase space has a periodic structure due to the standing-wave laser. The structure is less pronounced at large values of $|v|$ since the motion of these atoms causes them to average over the force which changes sign every $\Lambda/2$.

The simplest case for which the equations of motion can be solved analytically is the *impulse approximation*. In this limit, the laser pulse is so short ($\tau \to 0$) that the atoms remain stationary during the pulse. From Eq. (22), the velocity increment given to an atom in this case will be

$$v_f - v_i = \int_{-\infty}^{\infty} \frac{dv}{dt} dt \approx V \sin(2kx), \tag{27}$$

where v_i and v_f are the velocities of the atom before and after interaction with the standing wave. Analytical solutions for the final velocity probability density $p(v_f)$ exist for at least two initial velocity probability densities $p(v_i)$ in the impulse approximation. The simplest case, a δ function density centered at $v = \bar{v}_i$, gives [see Fig. 6(a)]

$$p(v_i) = \delta(v_i - \bar{v}_i) \to p(v_f) = \frac{1}{\pi} \frac{1}{\sqrt{V^2 - (v_f - \bar{v}_i)^2}}. \tag{28}$$

The matched pair of slits in our experiments produces an initial probability density that is triangular, and the final velocity probability density has a long functional form involving inverse trigonometric functions and square roots. Due to its length, we do not reproduce the solution here (see Ref. [11]). However, this case is graphically presented in Fig. 6(b).

In general, the equations of motion, Eq. (22), must be solved numerically. However, in the experiment the standing-wave-laser pulse is so short (τ= 3 ns) that the

error introduced by the impulse approximation is negligibly small compared to other error contributions. For an atom with a tensor polarizability, magnetic sublevels with differing values of $|m|$ will have different polarizabilities. This implies the existence of $J+1$ (J integral) or $J+1/2$ (J half-integral) different characteristic velocities for the magnetic sublevels. An equal number of equations of motion must be solved.

III. DETECTION OF THE LIGHT FORCE

To detect the effect of the light force, we measure the change in the velocity probability density $p(v)$. The velocity states of the atoms are probed using a cw laser tuned near resonance — typically within a natural linewidth. The probe laser beam intersects the atoms just downstream from the standing-wave laser beam — see Fig. 7. Atoms that received velocity kicks due to the light force are Doppler shifted *into* or *out of* resonance, thereby increasing or decreasing the absorption of light from the probe laser, respectively. For example, if the matched pair of slits prepared the atoms so that the mean value of the initial transverse velocity distribution was $\bar{v}_i = v_D$, then the light force would Doppler detune atoms *out of* resonance. (The velocity v_D corresponds to the transverse velocity required to tune atoms into resonance with the probe laser, whose frequency is slightly detuned from the rest-atom resonance frequency.) The probe light transmission would therefore increase, as is shown in the data plotted in Fig. 8. Since the standing-wave laser pulse is of short duration, only a small slice of atoms in the atomic beam are affected by it. As

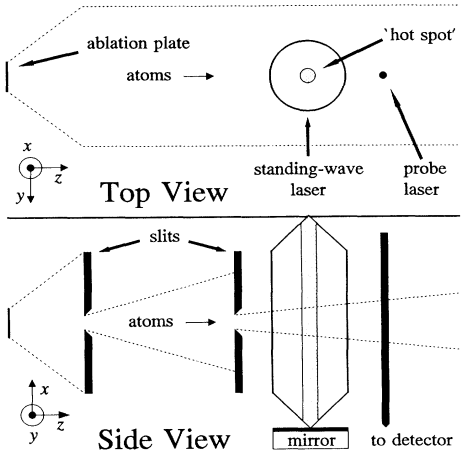

FIG. 7. A sketch of the experimental apparatus for measuring atomic polarizabilities. The atoms are produced at time $t = 0$ at the ablation plate. The atoms pass through two slits which limit motion in the x direction. At time t_{sw} the standing-wave laser fires, imprinting a change in the distribution of atoms in (x, v) phase space which depends on the position of the atoms with respect to "hot spots" in the standing-wave laser. The structure imprinted on the atoms is carried to the probe laser by the motion of the atoms in z. The probe laser sees a time-dependent velocity distribution due to the fluence distribution of the standing-wave laser.

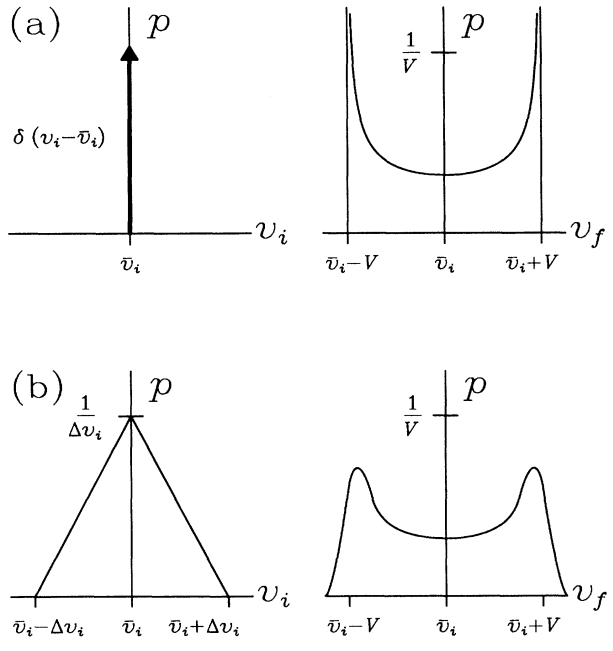

FIG. 6. (a) The initial and final velocity distributions for the δ-function initial velocity distribution of a perfectly collimated atomic beam. (b) The initial and final velocity distributions for the triangular initial velocity distribution formed by passing an atomic beam through a pair of slits of equal widths. The final velocity distribution is plotted here with $V = 4\Delta v_i$. In the limit $V/\Delta v_i \to \infty$ the final velocity distribution approaches that of (a).

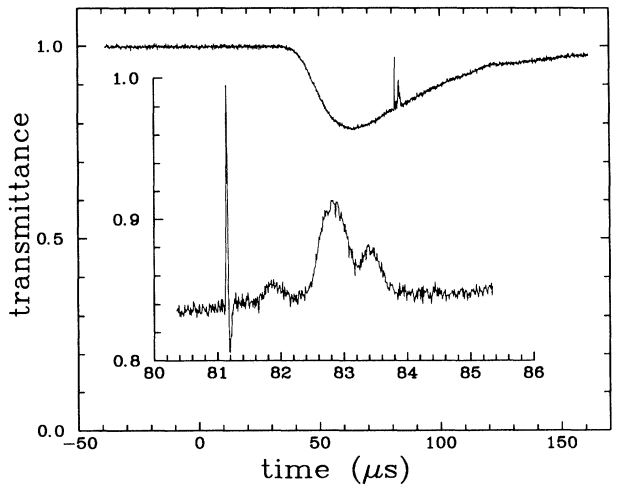

FIG. 8. A plot of the raw data for rubidium showing the transmittance of the probe laser as a function of time. Increased transmittance of the probe laser is visible as the broad feature with three peaks that occurs slightly later than the standing-wave pulse (the sharp spike at time=81.2 μs). This region is expanded in a plot in the lower left-hand corner.

a result, the probe laser light transmitted through the atomic beam has the temporal shape given in Fig. 8. The broad, large absorption feature is simply the absorption of the probe laser light as the atomic beam pulse passes through it. Within that feature is the sharp spike denoting when the standing-wave laser pulse was present. The feature that appears just after the standing-wave laser pulse spike is caused by the atoms that received velocity kicks from the light force. The transmittance increases after the standing-wave pulse because atoms have been shifted off resonance by the velocity kick supplied by the polarization force.

A. Absorption of the probe light

The ratio of the transmitted probe intensity I_p to the incident intensity I_0 is related to the absorption coefficient

$$a(\omega_p) = -\ln\left(\frac{I_p(\omega_p)}{I_0}\right), \tag{29}$$

where ω_p is the angular frequency of the probe light. In terms of the Doppler-shifted absorption cross section $\sigma(\omega_p, v)$ this coefficient can be written

$$a(\omega_p) = nl\int_{-\infty}^{+\infty}\sigma(\omega_p, v)p(v)dv, \tag{30}$$

where the column density of atoms is given by

$$nl = \int n(x)dx. \tag{31}$$

The quantity $n(x)$ is the number density (cm^{-3}) of atoms at position x. The integral in Eq. (30) serves to weight the cross section for atoms moving at the velocity v by their probability density in the beam. The absorption cross section $\sigma(\omega_p, v)$ for an atom moving with velocity v is

$$\sigma(\omega_p, v) = \frac{\sigma_0\Gamma\pi}{2}g_L(\omega_p, v). \tag{32}$$

Here σ_0 is the on-resonance cross section, Γ is the FWHM linewidth of the probe transition, and $g_L(\omega_p, v)$ is the normalized, Doppler-shifted Lorentzian line shape, that is

$$g_L(\omega_p, v) = \frac{\Gamma/2\pi}{(\omega_p - \omega_0 + k_p v)^2 + \Gamma^2/4}, \tag{33}$$

where ω_0 is the resonant frequency and k_p is the magnitude of the probe laser wave vector. Note that we choose the direction of the probe laser wave vector to be $\hat{\mathbf{k}}_p = -\hat{\mathbf{x}}$.

We introduce some notation to express the absorption coefficient in a form that is useful for interpreting experimental results. Since the probe laser frequency is fixed by locking the probe laser to an atomic line using saturated absorption or by locking the laser to an external Fabry-Pérot cavity, we shall no longer explicitly indicate the dependence of the absorption on ω_p. We express the velocity probability density not only as a function of velocity v, but also as a function of its mean initial velocity $\bar{v}_i$ and as a function of the characteristic velocity V. The dependence on V is a direct result of the light force. The probability density can now be written $p(v; \bar{v}_i, V)$, and with the help of Eqs. (30), (32), and (33) we can write the absorption coefficient for light at ω_p as

$$a(\bar{v}_i, V) = nl\frac{\sigma_0\Gamma\pi}{2} \times \int_{-\infty}^{+\infty}\frac{[p(v; \bar{v}_i, V)\Gamma/2\pi]dv}{(\omega_p + \omega_0 v/c - \omega_0)^2 + \Gamma^2/4}. \tag{34}$$

The absorption coefficient [Eq. (34)] is simply a convolution of the velocity distribution $p(v; \bar{v}_i, V)$ and a Lorentzian function of v. The absorption coefficient depends on the polarizability α through the characteristic velocity V.

B. Determining the polarizability α

The polarizability is found by measuring the absorption coefficient $a(\bar{v}_i, V)$ as a function of the mean velocity of the atoms $\bar{v}_i$ under conditions of nearly fixed V. Plots of the velocity distributions for various values of V are provided in Fig. 9. In Fig. 10 the absorption coefficient $a(\bar{v}_i, V)$ is plotted as a function of $\bar{v}_i$. Both the characteristic velocity V and the mean velocity $\bar{v}_i$ are given in units of the FWHM of the initial velocity distribution Δv_i. These absorption coefficient curves correspond to convolutions of a Lorentzian function of velocity with the final velocity distributions given in Fig. 9.

The absorption coefficient Eq. (34) depends linearly on column density nl. Experimentally, the column density fluctuates due to pulse-to-pulse variations in the atomic beam density and so it is essential to form a quantity which is independent of the column density. We define the "signal" S as

$$S(\bar{v}_i, V) = 1 - \frac{a(\bar{v}_i, V)}{a(\bar{v}_i, V = 0)}. \tag{35}$$

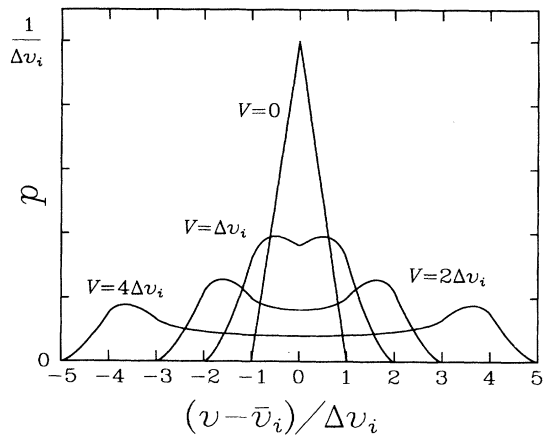

FIG. 9. The velocity distribution (in the impulse approximation) for an initial velocity distribution which is triangular, centered at $\bar{v}_i$ with a FWHM of Δv_i. The characteristic velocity V is proportional to the polarizability of the atoms and to the fluence of the standing-wave laser [see Eq. (21)].

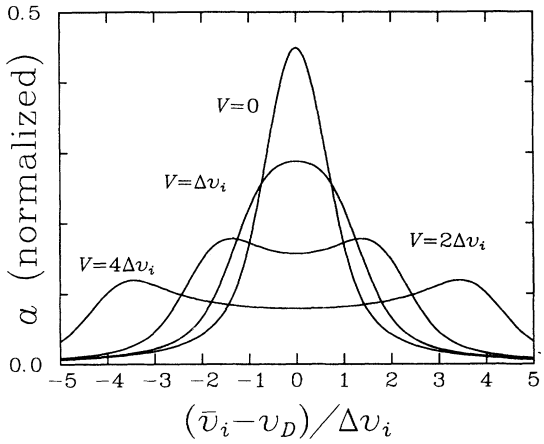

FIG. 10. The absorption distribution of atoms for the set of velocity distributions shown in Fig. 9. For illustration we have chosen the FWHM width of the Lorentzian Γ and the width of the initial velocity distribution Δv_i to be equivalent: $v_\Gamma = c\Gamma/\omega = \Delta v_i$ where ω is the frequency of the probe laser. The absorption a in this plot is normalized with respect to $(\bar{v}_i - v_D)/\Delta v_i$.

Several other quantities which are independent of the column density can be formed from the measured absorption coefficients. Three characteristics of S motivated us to choose to evaluate this particular combination of absorption coefficients:

(i) S is linear in $a(\bar{v}_i, V)$, the absorption coefficient of atoms which have been affected by the standing-wave laser.

(ii) $S = 0$ when the standing-wave laser has no effect.

(iii) $S > 0$ when the initial (field-free) absorption is a maximum. This occurs when $\bar{v}_i = v_D$ as is shown in Fig. 11. The effect of the standing-wave laser is to broaden the velocity distribution. As a result, the absorption is decreased at $\bar{v}_i = v_D$ by the effect of the standing wave, so that $S > 0$.

The signal S is plotted in Fig. 11 for the same values of

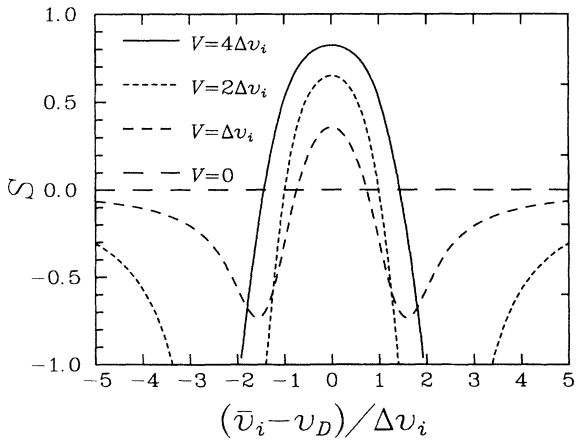

FIG. 11. The signal S plotted under the same conditions as the absorption distribution in Fig. 10.

the characteristic velocity V as the plots of the absorption coefficient in Fig. 10.

Since the signal S is the quantity which is measured in order to determine the polarizability, it is important to note the dependence of S on physical parameters of the experiment. The characteristic velocity depends linearly on the polarizability α and on the standing-wave laser fluence $\mathcal{F}$, and hence the signal also depends on these fundamental quantities. Since the standing-wave laser fluence depends on the (y, z) position of the atoms within the laser beam, the signal will also depend on these coordinates. The probe laser area is restricted through the use of an aperture so that the measured absorption corresponds to atoms that are located in a narrow region centered at the position of maximum fluence (see Fig. 7). We assume that during the time of the laser pulse the motion of an atom along y or z is small enough that the atom has experienced a uniform fluence, that is, a given atom does not sample different fluence regions of the laser beam. Even though this position remains fixed throughout the experiments, the fluence at this position varies from shot to shot due to overall changes in the pulse energy and spatial distribution. Hence the fluence at this fixed position is measured for each shot. Most of the parameters on which the signal depends remain *fixed* during the experiments. These include Δv_i, τ, ω_0, Γ, α, ω_p, and the position of the atoms within the standing-wave laser beam (y, z). The signal S is therefore a function of two parameters which vary for a set of data: the characteristic velocity V and mean initial velocity $\bar{v}_i$. The most physically meaningful way to express the signal is

$$S = S(\bar{v}_i, \alpha, \mathcal{F}) = 1 - \frac{a(\bar{v}_i, \alpha, \mathcal{F})}{a(\bar{v}_i, \alpha, 0)}, \tag{36}$$

where the dependence on characteristic velocity has been split up to indicate the explicit dependence of S on the atomic polarizability α and on the laser fluence $\mathcal{F}$. Data are taken by selecting an initial mean velocity $\bar{v}_i$, and by simultaneously measuring three quantities: (i) $\mathcal{F}_{\max}$, the fluence at the position of maximum fluence, (ii) $a(\bar{v}_i, \alpha, \mathcal{F}_{\max})$, the absorption coefficient for atoms affected by the light force at the same position; and (iii) $a(\bar{v}_i, \alpha, 0)$, the absorption coefficient for the same atoms in the absence of the light force, deduced by extrapolating field-free regions of the absorption curve. The polarizability is found by fitting the signal versus mean velocity data with the polarizability α as a parameter that is varied to obtain the best fit to the theory. An example of this procedure will be presented in Sec. IV for the case of rubidium.

The mean atomic velocity is determined by the position of the second slit relative to the first slit as shown in Fig. 12. The slit position can be accurately transformed into a mean transverse velocity $\bar{v}_i$ in the following way. Define the distance from the first slit to the second slit (parallel to the atomic beam propagation axis) as z_{ss} — see Fig. 12. Define the longitudinal velocity of the atoms to be v_z. From geometry, the mean transverse velocity $\bar{v}_i$ of the atoms passing through a slit displaced a distance

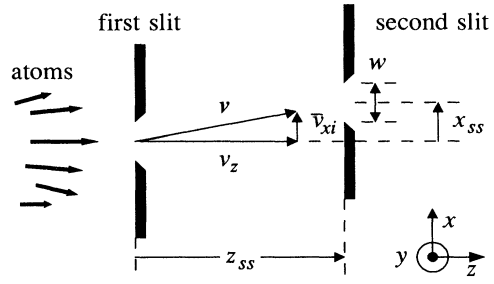

FIG. 12. Geometry of the atomic beam slits.

x_{ss} from the centerline position of the atomic beam is

$$\frac{\bar{v}_i}{v_z} = \frac{x_{ss}}{z_{ss}}. \tag{37}$$

Thus the slit position is related to the mean transverse velocity by a constant factor that can be easily and accurately measured. For convenience, the abscissa (velocity axis) of the absorption coefficient curves is scaled to a physical velocity that is determined by the initial velocity distribution. The FWHM of the initial, triangular velocity probability density Δv_i is determined by the slit width w. Again from geometry, it can be shown that

$$\frac{\Delta v_i}{v_z} = \frac{w}{z_{ss}}. \tag{38}$$

From this and Eq. (37) the following result can be derived:

$$\frac{\bar{v}_i}{\Delta v_i} = \frac{x_{ss}}{w}. \tag{39}$$

Hence all plots of the absorption coefficient versus mean transverse velocity (or slit position) are scaled by Δv_i (or by w).

C. Modifications for measuring a tensor polarizability

Thus far we have only considered detection of atoms with a scalar polarizability. For atoms with angular momentum $J > 1/2$, the polarizability is a tensor and different magnetic sublevels will have different values of the polarizability — see the Appendix. In general, three quantities completely specify the polarizability tensor of an atom: the scalar polarizability α_0, the vector polarizability α_1, and the tensor polarizability α_2. However, if linearly polarized light is used for the light force, only two components α_0 and α_2 are important. These are also the only components measurable using static fields. For example, defining the polarization axis of the standing-wave laser as the quantization axis, it is the α_{zz} component of the polarizability tensor that is important in the light force — see Eq. (A9). Using this equation, the diagonal terms of this component of the polarizability tensor for an atom of angular momentum J in sublevel m can be written

$$\alpha_{zz}(m) = \alpha_0 + \alpha_2 \frac{[3m^2 - J(J+1)]}{J(2J-1)}. \tag{40}$$

The polarizability depends on the square of the magnetic sublevel quantization number, i.e., $\alpha_{zz}(m) = \alpha(|m|)$. This dependence of α on $|m|$ will cause the light force to produce either $J + 1$ (J integral) or $J + 1/2$ (J half-integral) final velocity distributions. Sublevels with larger α's will experience larger kicks and hence their final velocity distributions will be broader and shallower than sublevels with smaller values of α. However, depending on the transitions used by the probe light, some of the sublevels might not contribute to the absorption. For example, if the probe laser is linearly polarized along $\hat{z}$ and the upper level angular momentum $J' = J - 1$, then the $m = \pm J$ sublevels of the ground state will not be probed, since Δm=0 for transitions involving light polarized along the quantization axis. Thus the absorption coefficient for a multilevel atom will have a form corresponding to the sum of expressions similar to Eq. (34), that is

$$a(\bar{v}_i, V) = \frac{nl}{2J+1}\frac{\Gamma\pi}{2}\sum_{m=-J}^{+J}\int_{-\infty}^{+\infty}\frac{\sigma_0(|m|)[p(v;\bar{v}_i,V(|m|))\Gamma/2\pi]dv}{(\omega_p+\omega_0 v/c-\omega_0)^2+\Gamma^2/4}. \tag{41}$$

This expression assumes that $\omega_R T \ll 1$, where ω_R is the Rabi flopping frequency of the probe laser-atom system and T is the time an atom spends in the laser probe beam. This condition ensures that optical pumping effects due to the probe laser beam are ignorable. If optical pumping were significant, then the absorption coefficient expression Eq. (41) would have to be modified to account for the different populations of the various sublevels. This expression also assumes that the probe laser intensity is less than the saturation intensity

$$I_{\text{sat}} = \frac{\hbar\omega_p}{2\sigma\tau_a}, \tag{42}$$

where τ_a is the lifetime of the upper level of the atomic transition and σ is the absorption cross section. At the saturation intensity the excitation rate equals the decay rate of the upper level. This avoids the added complication of having to account for the dependence of the linewidth Γ on intensity I and on magnetic sublevel m. The expression Eq. (41) assumes a statistical distribution of the atoms among the magnetic sublevels.

D. Limitations of absorption for detection

There are several limitations to absorption as a method for detecting the light force. One limitation is the probe

laser intensity must be limited to prevent line broadening effects in the absorption line shape and to prevent optical pumping effects that can modify the probability distribution. This means that the probe laser intensity must be kept below the saturation intensity of the transition used to measure the absorption. Two limitations occur if the probe transition is weak: the absorption will be small, reducing the signal-to-noise ratio; and the line will be narrow, so locking the probe laser frequency on resonance will be more technically challenging. A third limitation can occur if there are several levels that lie below the upper level of the selected probe transition. Then atoms can branch into lower levels other than the ground state. However, this limitation is unimportant as long as the probability that an atom scatters light is low. This condition implies $\omega_R T \ll 1$. If an atom with significant tensor polarizability components has hyperfine structure, this complicates the analysis of the absorption coefficient Eq. (41). A full treatment of the light force for isotopes that fall into this category awaits future analysis. In Sec. 5 of the Appendix there is a brief discussion on the tensor polarizability when hyperfine structure is present. As already noted, atoms with scalar polarizabilities in the absence of hyperfine structure will remain scalar to a very good approximation due to the small size of the hyperfine interaction. The alkali-metal atoms are an excellent example of this class of atoms. Another limitation to the absorption probe is that most atoms have principal lines in the ultraviolet region, which is technically more difficult to access with lasers. Although nonlinear optical techniques have made this region very accessible for pulsed laser sources, tunable cw lasers are not intense enough to obtain good nonlinear conversion efficiency from the visible to the ultraviolet.

IV. APPLICATION TO RUBIDIUM

To establish the viability and accuracy of our technique [7], we applied it to rubidium, whose polarizability has been accurately measured by the *E-H* gradient balance technique [3]. Rubidium has a scalar polarizability that dominates the other terms of the polarizability tensor by seven orders of magnitude. The small tensor component α_2, which arises from the small energy differences that result from the hyperfine interaction, has also been measured [14].

The experimental setup was as follows. A beam of rubidium atoms was produced using two-stage laser-ablation [15] of a solid Na-Rb target with Nd:YAG laser pulses of energy E=100 mJ and of duration $\Delta\tau = 10$ ns. The target was composed of roughly equal parts of sodium and rubidium. The purpose of the sodium in the target was to form a rubidium mixture whose oxidized surface would not continually dissolve into the metal target during preparation. The atomic beam was produced at a repetition rate of 0.4 Hz (12 ablation pulses were used in first-stage loading of the target). The first slit was located 13 cm from the target and the second slit was downstream 13 cm from the first slit. Both slits were identical, commercially made slits of width 280 μm. The mean longitudinal velocity of the beam was 3.6×10^5 cm/s and the beam pulse was of 50 μs duration. The standing-wave laser was an injection-seeded Nd:YAG laser with a peak fluence of 3 J/cm^2, a FWHM pulse duration of 7 ns, and a coherence length of 2 m — close to the Fourier transform limit. The laser beam was oriented so that its (linear) polarization axis was parallel to the $\hat{z}$ axis. The center of the standing-wave laser was located 4 cm downstream from the second slit. The probe laser was a single-mode diode laser that utilized an external-grating cavity to tune it close to resonance. It produced 1 mW of light with a linewidth of $\lesssim 1$ MHz. This laser was detuned $\nu_d = (\omega_p - \omega_0)/2\pi = 5.0$ MHz from the F=3 to 4 transition of the D_2 line of ^{85}Rb. The diode laser was locked at this frequency using a saturated absorption setup with a cell of rubidium atoms. The probe laser intersected the atomic beam 0.6 cm downstream from the standing-wave laser. The diode laser light was linearly polarized parallel to the standing-wave polarization axis.

The probe laser light detected by the photodetector sampled only those atoms that traversed the region of maximum fluence. Achieving this condition was not trivial due to the shot-to-shot pointing variations in the standing-wave laser. We selected only those pulses whose position stayed within 150 μm of the "best" position, i.e., the position corresponding to the center of the fluence maximum lining up with the center of the probe aperture. The distance 150 μm corresponds to half the radius of the probe aperture. This was accomplished by directing a small fraction of the standing-wave beam on each pulse to a quad-cell photodetector. A digital oscilloscope was only triggered, and data accepted, if the quad-cell photodetector indicated the shot was within the acceptable range of pointing directions. Roughly half the shots were accepted using this technique, although small adjustments (< 1mrad) of the direction of the standing-wave beam were required during data runs.

The raw data consisted of the probe transmittance versus time — see Fig. 8. These plots represent the average of 20 pulses, taken with a digital oscilloscope. Two pieces of data were extracted from each curve. First, the absorption coefficient was measured at the time the light force was a maximum — label this $a(\bar{v}_i, \alpha, \mathcal{F}_{\max}) \equiv a(\mathcal{F}_{\max})$. Second, the absorption coefficient in the field-free regime was measured at the time of the occurrence of the light force maximum — label this $a(\bar{v}_i, \alpha, 0) \equiv a(0)$. The field-free absorption $a(0)$ at the time of the light-force peak was deduced by interpolating the field-free portions of the curve. Both absorption quantities are functions of the slit position and they both gradually fall to zero as the slit is translated to allow higher transverse velocities through. A figure of merit for the size of the force is the ratio $a(\mathcal{F}_{\max})/a(0)$, which reached a maximum value of 0.5. This implies that the polarization force gave half the atoms a velocity kick large enough to Doppler shift their resonant frequencies away from their stationary-atom values.

Many curves similar to Fig. 8 were taken for various slit positions, which correspond to different values for the mean velocity $\bar{v}_i$. Data for the absorptions $a(\mathcal{F}_{\max})$ and $a(0)$ as a function of mean transverse velocity $\bar{v}_i/\Delta v_i$ for

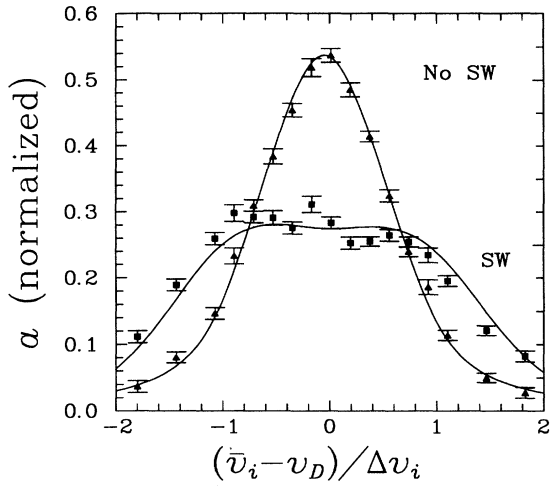

FIG. 13. Experimentally measured values of the absorption, normalized by a reference absorption probe in order to remove fluctuations in the atomic beam density. The initial velocity distribution is fit by varying the center and vertical scale of the curve. The final velocity distribution is fit with values of these parameters fixed at the values used to fit the initial velocity distribution. A quantity proportional to the polarizability is the only parameter varied in order to fit the normalized absorption for atoms affected by the standing wave. On the figure the abbreviation "SW" means the standing-wave beam was present and "No SW" means it was absent.

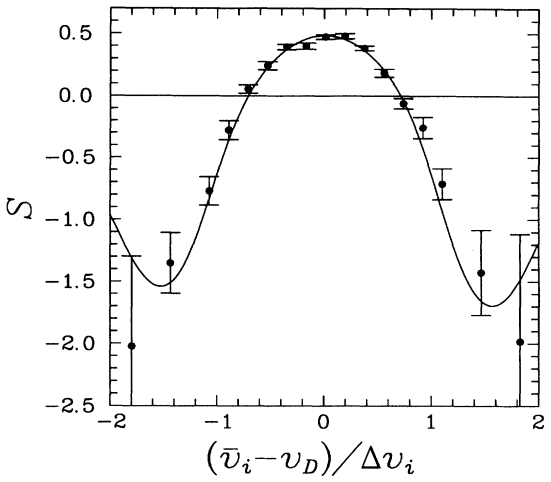

FIG. 14. The experimentally determined signal S vs mean initial velocity $\bar{v}_i$, and the fit to this data. There are only two fit parameters: the center of the curve and a parameter which is proportional to the polarizability.

rubidium are given in Fig. 13. Also included are best-fit curves for both sets of data. As discussed in Sec. III, these curves physically correspond to the transverse velocity distributions convoluted with a Lorentzian line shape. The first curve displays the field-free absorption distribution, which corresponds to a convolution of a triangle distribution with a Lorentzian line shape. It is clear that the agreement between the data and the theoretical curve is quite good. This plot of absorption coefficients versus mean velocity $\bar{v}_i$ has had each point normalized for number density variations by the signal generated by intersecting a small amount of the probe laser light with the atoms just before the atoms encounter the second slit. Without this normalization, the data are much noisier [11]. A better normalization procedure is to generate the signal S as discussed earlier. A plot of S versus mean velocity $\bar{v}_i$ for rubidium is given in Fig. 14. The curve through the data points represents a best fit of the theory to the data. We obtain a value for the polarizability from our fit to the signal data (S versus $\bar{v}_i$). The expression used to obtain a value of α from the measured quantities is

$$\alpha(\omega) = \left(\frac{M\lambda c}{16\pi^2}\right) \frac{V' \Delta v_i}{\mathcal{F}}. \tag{43}$$

The terms in parentheses constitute an accurately known constant. The FWHM of the velocity distribution Δv_i is determined from the geometry of the slits and by measuring the longitudinal velocity of the atoms at the position of the standing-wave laser. The quantity V' is obtained from the fit like that shown in Fig. 14. It corresponds to the scaled characteristic velocity, i.e., $V' = V/\Delta v_i$.

The fluence of the standing-wave laser and the transmittance of the probe laser are measured simultaneously. A small amount of light is diverted from the standing-wave laser beam to an energy meter. The standing-wave laser beam has significant spatial structure (see Fig. 15). Therefore an aperture of area A is inserted in front of the energy meter to select the region of maximum fluence. An identical aperture is inserted into the path of the probe laser after it has propagated through the atomic beam, in order to select atoms which have traversed the region of maximum fluence. Both apertures are scanned for maximum signal to locate their positions. We define T to be the ratio of the fluence at the energy meter aperture to the fluence at the standing-wave laser mirror. We then calculate the fluence as $\mathcal{F} = E/(AT)$, where E is the energy deposited on the energy meter.

The best fit to the data shown in Fig. 14 gives a value for the polarizability of $\alpha(\omega) = 114 \pm 9$ Å^3. The quoted error is an estimate of the standard deviation uncertainty in our value of $\alpha(\omega)$ based on error in the quantities $\mathcal{F}$ (7.6%), V' (2.2%), and Δv_i (1.6%). The major factors contributing to the fluence error are the uncertainty in the location of the energy meter aperture with respect to the peak fluence region of the standing-wave laser beam (6%) and the uncertainty in the location of the probe laser aperture with respect to atoms that traversed the peak fluence region (4%).

To find the static polarizability $\alpha_{\rm dc}$, a value for the ratio $r = \alpha(\omega)/\alpha_{\rm dc}$ must be determined — see the Appendix. A simple and convenient expression for the frequency-dependent polarizability in terms of oscillator strengths can be derived [see Eq. (A10)]

$$\alpha(\omega) = \frac{e^2}{m_e} \sum_k \frac{f_k}{(\omega_k^2 - \omega^2)}. \tag{44}$$

This expression applies at large detunings from all atomic

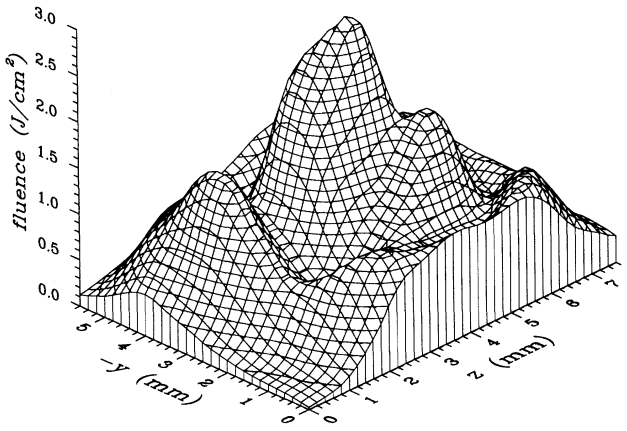

FIG. 15. Three-dimensional plot of the fluence distribution of the standing-wave laser. The mean atomic velocity is in the $+\hat{\mathbf{z}}$ direction and the standing-wave mirror normal is in the $+\hat{\mathbf{x}}$ direction ("up" in this figure).

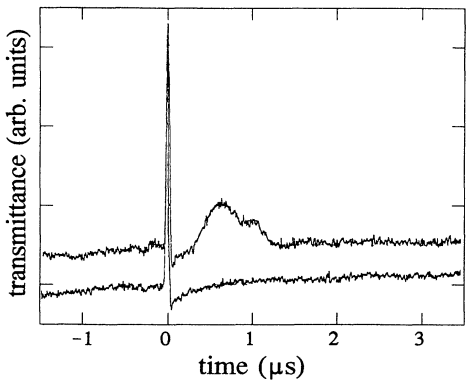

FIG. 16. Raw data showing the effect of widening the second slit. The two curves shown above were taken a few minutes apart. In the upper curve, the first and second slits have a width of 250 μ. In the lower curve, the second slit has been opened to 1000 μ. The origin of time is chosen to be when the standing-wave laser fires. The vertical scale has been adjusted so that the height of the sharp peak, observed when the standing wave is present, is the same for both curves. (The sharp peak is proportional to the initial absorption.) The vertical displacement between the curves is arbitrary.

resonance frequencies. The symbol **S** indicates summation over discrete states and integration over continuum states — see the Appendix. This expression gives the value $r = 2.12$ using the rubidium oscillator strengths published by Shabanova and Khlyustalov [16] and the continuum cross sections published by Marr and Creek [17]. Scaling our measured value for the polarizability at ω by this ratio gives an estimate for the static polarizability of $\alpha = 54 \pm 4$ Å^3, where the error does not include any error in the value of r. This value is within 15% of the accepted value of $\alpha = 47.3 \pm 0.9$ Å^3 (2σ), measured by Molof *et al.* [3]. It is possible, though unlikely, that our value is too high compared to the accepted value due to the inaccuracy of the ac correction, r. The Appendix discusses the insensitivity of r to the values used for the oscillator strengths in Eq. (44).

In general, the need to convert an ac polarizability to a static polarizability using a calculated value for r is not a significant limitation to the light-force technique. Most atoms require much smaller corrections since their resonance lines are much farther detuned from the Nd:YAG frequency than those of rubidium. Also, using standing-wave lasers at two different frequencies would allow better extrapolation of the measured ac polarizability to the dc value. Alternatively, the light-force technique could be applied using a CO_2 laser, whose wavelength ($\lambda = 10.6$ μm) is a factor of 10 longer than that of Nd:YAG. For rubidium the correction would then be $r = 1.005$.

One other experimental result is worth examining. In Fig. 16, the transmittance of the laser probe is plotted versus time for two different situations. In this case the second slit was adjustable; the first slit was fixed at a gap of $w_1 = 250$ μm. For the upper curve, the second slit width was $w_2 = 250$ μm, and the data show the expected increase in transmittance present in the case of the fixed slits. However, for the lower curve the second slit was opened to $w_2 = 1000$ μm, and the transmittance was not affected by the light force that was present when the standing-wave laser was fired. This is simply a result of Liouville's theorem, where the wider slit has essentially made the atomic phase space uniformly dense and so the conservative light force cannot affect the phase-space distribution. This result also confirms that the increased transmittance present in the upper curve is due to the light force and not due to ionization or excitation of atoms out of the ground state.

V. CONCLUSION

This paper has discussed a method called the light-force technique, which was specifically designed to determine electric-dipole polarizabilities for refractory-metal atoms. Expressions for the light force have been derived and discussed in detail. The effect of the light force on atoms that have significant polarizability tensor components has also been presented. The light force, which produces a redistribution of atoms in phase space, is detected by measuring the absorption of a probe laser beam tuned to an atomic resonance. The detection of the light force by absorption has been thoroughly discussed. Finally, successful application of the technique to a measurement of the polarizability of rubidium has also been reviewed.

The technique is limited in several ways. The size of the light force is limited by the need to keep the standing-wave laser intensity low enough to avoid excitation and ionization of the atoms. Also, the need to maintain coherence lengths of 1 cm or more limit the temporal pulsewidth of the standing-wave laser to times larger than a few picoseconds. Since absorption of cw

laser light by the atoms is used to detect the light force, the intensity of the cw laser light must be limited to minimize line broadening and optical pumping effects.

The technique takes advantage of the large fields and field gradients that modern pulsed lasers are capable of producing. Also, the atomic beam is pulsed in order to naturally match the light-force laser and to increase the atomic density over that achievable with traditional beam sources. The light-force technique provides an *absolute* measurement of the polarizability. The measured polarizability is the atomic polarizability at the frequency of the standing-wave laser. In many cases the correction required to determine the static polarizability is small and may be easily and accurately calculated using published values of oscillator strengths and transition frequencies.

ACKNOWLEDGMENTS

The authors are grateful to Will Happer for his support and encouragement of this work. We also thank Thad Walker for many helpful discussions and we thank Carl Collins for technical help. This work was supported by DOE Grants Nos. LLNL/DOE/C 1133303 and LLNL/DOE B150385 and by the Army Research Office, Grant No. DAAL-87-K-0068.

APPENDIX: THE POLARIZABILITY α

1. General properties

The frequency-dependent polarizability can be described in terms of three complex functions of frequency: the scalar polarizability α_0, which describes the index of refraction of a vapor of atoms with randomly oriented spin directions; the vector polarizability α_1, which can be nonzero if $J > 0$ and which describes physical phenomena like the paramagnetic Faraday rotation of plane polarized light by spin polarized atomic vapors; and the tensor polarizability α_2, which can be nonzero for $J > 1/2$ and which describes the birefringence of a vapor of spin-aligned atoms. The frequency-dependent polarizability operator can be written in terms of the electronic angular momentum operators $\hat{J}_i$ of the atom as

$$\hat{\alpha}_{ij} = \alpha_0 \hat{\delta}_{ij} - \alpha_1 (\hat{J}_i \hat{J}_j - \hat{J}_j \hat{J}_i) + \alpha_2 \frac{\frac{3}{2}(\hat{J}_i \hat{J}_j + \hat{J}_j \hat{J}_i) - J(J+1)\hat{\delta}_{ij}}{J(2J-1)}. \quad \text{(A1)}$$

Here the indices ij refer to Cartesian components as discussed in Sec. II and $\hat{\delta}_{ij} = \delta_{ij}\hat{I}$, where δ_{ij} is the Kronecker delta function and $\hat{I}$ is the identity operator.

In the case of atoms with degenerate ground states we note that $\alpha_1 \to 0$ as $\omega \to 0$ (see the expression for α_1 below), so the vector polarizability will be negligible compared to the scalar and tensor polarizabilities at sufficiently low oscillation frequencies ω. It is also true that the anti-Hermitian part of $\boldsymbol{\alpha}(\omega)$ approaches zero as the frequency goes to zero. The polarizability at low frequencies will therefore be very nearly a real, symmetric tensor.

The complex coefficients α_i in Eq. (A1) do not depend on the particular magnetic sublevel m of the ground state, since the dependence of $\hat{\alpha}_{ij}$ on geometry is given by the angular momentum operators explicit in Eq. (A1). Expressions for these coefficients can be found using first-order time-dependent perturbation theory [18]. In the limit of large detuning from resonance, these coefficients have the following values

$$\alpha_0 = \frac{2}{3\hbar g_J} \mathbf{S}_{k\neq\mu} \frac{\phi_0(J,J_k)\omega_{k\mu}}{(\omega_{k\mu}^2 - \omega^2)} |\langle \gamma_\mu J||\hat{p}||\gamma_k J_k\rangle|^2,$$
$$\alpha_1 = \frac{1}{\hbar g_J} \mathbf{S}_{k\neq\mu} \frac{\phi_1(J,J_k)\omega}{(\omega_{k\mu}^2 - \omega^2)} |\langle \gamma_\mu J||\hat{p}||\gamma_k J_k\rangle|^2, \quad \text{(A2)}$$
$$\alpha_2 = \frac{2}{3\hbar g_J} \mathbf{S}_{k\neq\mu} \frac{\phi_2(J,J_k)\omega_{k\mu}}{(\omega_{k\mu}^2 - \omega^2)} |\langle \gamma_\mu J||\hat{p}||\gamma_k J_k\rangle|^2,$$

where $g_J = 2J+1$ is the degeneracy of the ground state and the functions $\phi_i(J,J_k)$ are defined as follows

$$\phi_0(J,J_k) = \delta_{J_k,J-1} + \delta_{J_k,J} + \delta_{J_k,J+1},$$

$$\phi_1(J,J_k) = \frac{1}{J(2J-1)}\delta_{J_k,J-1} + \frac{1}{J(J+1)(2J-1)}\delta_{J_k,J} - \frac{1}{J+1}\delta_{J_k,J+1}, \quad \text{(A3)}$$

$$\phi_2(J,J_k) = -\delta_{J_k,J-1} + \frac{2J-1}{J+1}\delta_{J_k,J} - \frac{J(2J-1)}{(J+1)(2J+3)}\delta_{J_k,J+1}.$$

Here the δ's are Kronecker delta functions. The symbol **S** denotes summation over discrete states and integration over continuum states; this symbol is used in standard physics texts [19] as well as in discussions of polarizabilities (see Dalgarno [20]). In the ground-state wave functions $|\gamma_\mu J\rangle$ the quantity γ_μ represents a set of ground-state quantum numbers (including, for example, the energy) and J is the ground-state angular momentum. Excited-state wave functions are similarly written $|\gamma_k J_k\rangle$, where γ_k represents a set of excited-state quantum numbers and J_k is the total angular momentum of the kth excited state. The operator $\hat{p}$ in the matrix elements above corresponds to the magnitude of the electric-dipole operator

$$\hat{\mathbf{p}} = \sum_{l=1}^{n} e\hat{\mathbf{r}}_l, \quad \text{(A4)}$$

where $\hat{\mathbf{r}}_l$ is the position operator of the lth electron in the atom. The frequencies $\omega_{k\mu}$ correspond to differences in the Bohr frequencies of the excited and ground states:

$$\omega_{k\mu} = (E_k - E_\mu)/\hbar, \quad \text{(A5)}$$

where E_i is the energy of the ith atomic level. The matrix elements $|\langle \gamma_\mu J||\hat{p}||\gamma_k J_k\rangle|^2$ are the usual reduced matrix elements associated with the Wigner-Eckart theo-

rem. According to the Wigner-Eckart theorem, the matrix element of a tensor operator, e.g., the qth component of the vector operator $\hat{\mathbf{p}}$, can be written as the product of a reduced matrix element and a geometric factor (Clebsch-Gordan coefficient or 3-j symbol)

$$\langle \gamma_\mu J m|\hat{p}_q^1|\gamma_k J_k m_k\rangle = \frac{(J_k m_k, 1q|JM)}{(2J+1)^{1/2}}\langle \gamma_\mu J||\hat{p}||\gamma_k J_k\rangle. \tag{A6}$$

Here the quantity $(J_k m_k, 1q|JM)$ is a Clebsch-Gordan coefficient [21]. The reduced matrix elements $\langle \gamma_\mu J||\hat{p}||\gamma_k J_k\rangle$ are related to the matrix elements used in the expressions of Miller and Bederson [5] $|\langle\psi_0|p|\psi_k\rangle|$ in the following way:

$$|\langle \gamma_\mu J||\hat{p}||\gamma_k J_k\rangle|^2 = \eta(J, J_k)(2J+1)|\langle\psi_0|p|\psi_k\rangle|^2, \tag{A7}$$

where the factor $\eta(J, J_k)$ is given by

$$\eta(J, J_k) = \delta_{J-1,J_k} J(2J-1) + \delta_{J,J_k} J(J+1) + \delta_{J+1,J_k}(2J+3)(J+1). \tag{A8}$$

In addition, the notation adopted here is slightly different from that of Miller and Bederson [5]. In their notation, the scalar polarizability α_0 is labeled the average polarizability $\bar{\alpha}$ to reflect the physical fact that the scalar polarizability is simply the average of the polarizability tensor over the magnetic sublevels m. In their notation the tensor polarizability α_2 is labeled α_t.

The diagonal terms of the polarizability operator Eq. (A1) in the large detuning limit are given by

$$\langle Jm|\hat{\alpha}_{ij}|Jm\rangle = \alpha_0\delta_{ij} - im\alpha_1\varepsilon_{ijk}\delta_{kz} + \alpha_2\frac{[3m^2 - J(J+1)]}{J(2J-1)}\delta_{ij}\left(-\frac{1}{2}\right)^{(1-\delta_{iz})}, \tag{A9}$$

where ε_{ijk} is the Levi-Civita antisymmetric tensor defined by

$$\varepsilon_{ijk} = \begin{cases} 1 & \text{if } ijk \text{ is cyclic in xyz} \\ 0 & \text{otherwise.} \end{cases}$$

In the dc limit, the coefficients α_i substituted into expression Eq. (A9) reproduce the results given by Miller and Bederson [5].

2. The scalar polarizability α_0

When the laser frequency is much smaller than any of the resonant frequencies, the scalar polarizability can be approximated by the expression

$$\alpha_0(\omega) = \frac{e^2}{m_e}\mathop{\mathbf{S}}_{k\neq\mu}\frac{f_{\mu k}}{(\omega_{k\mu}^2 - \omega^2)}. = \frac{e^2}{m_e}\left[\sum_{k\neq\mu}\frac{f_{\mu k}}{(\omega_{k\mu}^2-\omega^2)} + \int_{\omega_{IP}}^{\infty}\frac{(df/d\omega')d\omega'}{[(\omega'-\omega_\mu)^2-\omega^2]}\right]. \tag{A10}$$

Here $f_{\mu k}$ is the absorption oscillator strength of the $\mu \rightarrow k$ transition

$$f_{\mu k} = \frac{2m_e\omega_{k\mu}}{3\hbar g_J e^2}|\langle \gamma_\mu J||\hat{p}||\gamma_k J_k\rangle|^2, \tag{A11}$$

and the lower limit on the integral corresponds to the Bohr frequency of the ionization potential. The continuum oscillator strength at the frequency ω is related to the photoionization cross section at the same frequency $\sigma(\omega)$ in the following way [22]:

$$\frac{df}{d\omega} = \frac{m_e c}{\pi e^2}\sigma(\omega), \tag{A12}$$

where c is the speed of light. In Eq. (A10) the shift in resonant frequency due to the motion of the atom has been ignored. This result is the same as the expression given in Eq. (A2) for the coefficient α_0, except that this form utilizes the oscillator strengths $f_{\mu k}$ of electric-dipole-allowed transitions with the ground state. This expression is an excellent approximation for the scalar polarizability for light at the Nd:YAG frequency. For example, for one of the worst cases — cesium — the Nd:YAG detuning from the nearest resonance is 55 THz.

To extract a value for the *static* or dc scalar polarizability $\alpha_0(dc)$ in the light-force experiments, the ratio $r_0 = \alpha_0(\omega_{sw})/\alpha_0(dc)$ must be known, where ω_{sw} is the Nd:YAG frequency. For the alkali metals, e.g., rubidium, the polarizability is a scalar and only the ratio r_0 is relevant. For rubidium the ratio is calculated to be 2.12. The frequency-dependent polarizability calculated from Eq. (A10) gives a value for rubidium of 47.2 Å^3, which agrees within experimental error with the value measured by Molof *et al.* [3]. This estimate of the polarizability was made using the oscillator strengths of Shabanova and Khlyustalov [16] and the photoionization cross sections of Marr and Creek [17].

3. The tensor polarizability α_2

We can write the tensor part of the polarizability using expressions similar to those provided in the preceding section for the scalar polarizability. We concentrate on expressions that apply at large detunings. In terms of oscillator strengths, the tensor part of the polarizability α_2 can be written [see Eq. (A2)]

$$\alpha_2(\omega) = \frac{e^2}{m_e}\mathop{\mathbf{S}}_{k\neq\mu}\frac{f_{\mu k}}{(\omega_{k\mu}^2-\omega^2)}\ \phi_2(J, J_k), \tag{A13}$$

where the angular momentum factor $\phi_2(J, J_k)$ is given in Eq. (A3). To extract a value for the *static* or dc tensor polarizability $\alpha_2(dc)$ in the light-force experiments, the ratio $r_2 = \alpha_2(\omega_{sw})/\alpha_2(\mathrm{dc})$ must be evaluated.

4. The sensitivity of the ratio r to oscillator strength values

The light-force technique relies on a knowledge of the ratios r_i to convert the measured ac components of the polarizability to their dc values. In turn, these ra-

tios depend on a knowledge of the absorption oscillator strengths $f_{\mu k}$ for transitions from the ground state to excited levels, as well as a knowledge of the photoionization cross section $\sigma(\omega)$. The ratios r_i are not as sensitive to the values used for the oscillator strengths and photoionization cross sections as one might expect. For example, the ratios are nearly independent of $\sigma(\omega)$ and the $f_{\mu k}$'s if a few lines dominate, as is the case for the alkali-metal atoms. Note that it is the accuracy of relative, not absolute, oscillator strengths that matters: if $\sigma(\omega)$ and all the $f_{\mu k}$'s were scaled by the same factor, the ratios r_i would remain unchanged.

For a sufficiently long-wavelength laser, we may assume that the contribution of the continuum to the polarizability will be the same at the frequency ω as at dc. An estimate for the rms error s_{r_i} of the ratio r_i is then

$$s_{r_i}^2 = \sum_k \left(\frac{\partial r_i}{\partial f_{\mu k}}\right)^2 s_{f_{\mu k}}^2 + (1-r_i)^2 \left(\frac{s_{\alpha_{ci}}}{\alpha_i(\mathrm{dc})}\right)^2, \quad \text{(A14)}$$

where $s_{f_{\mu k}}$ is the rms uncertainty in the value of the kth oscillator strength, and $s_{\alpha_{ci}}$ is the rms uncertainty of the contribution of the continuum to the α_ith component of the polarizability of the atom. This expression assumes the uncertainties in α_c and the $f_{\mu k}$'s are uncorrelated. For example, using this expression to estimate the error in the value of r_0 for rubidium gives $s_{r_0} = 1.4 \times 10^{-2}$. For the alkali metals, like rubidium, the sensitivity of r to the large uncertainties (roughly 20%) in the continuum oscillator strengths is weak. However, for other atoms, such as the inert gases, where a significant fraction of the polarizability is contributed by continuum transitions, a good estimate of the ratio r requires good data on the photoionization cross section as a function of frequency. When accurate data are not available, accurate measurements of r can still be made at long wavelengths, where $r \approx 1$ and $(1-r)^2 \ll 1$.

5. Atomic polarizability and hyperfine structure

For atoms that have nonzero nuclear spin I, the hyperfine interaction must be accounted for in the zeroth-order Hamiltonian, i.e., when there is no external electric field. Here, the total angular momentum $F = J + I$ and the projection of the total angular momentum along the quantization axis $F_z = J_z + I_z$ are good quantum numbers and the eigenvectors can be labeled $|\gamma F M_F\rangle$.

The frequency-dependent polarizability operator can be written in terms of the total angular momentum operators F_i of the atom as

$$\hat{\alpha}_{ij} = \alpha_0 \hat{\delta}_{ij} - \alpha_1 (\hat{F}_i \hat{F}_j - \hat{F}_j \hat{F}_i) + \alpha_2 \frac{\frac{3}{2}(\hat{F}_i \hat{F}_j + \hat{F}_j \hat{F}_i) - F(F+1)\hat{\delta}_{ij}}{F(2F-1)}. \quad \text{(A15)}$$

The expressions for the coefficients α_i are exactly identical to those given in Eqs. (A2) and (A3) with the transformations $J \to F$ and $J_k \to F_k$.

When the hyperfine interaction is weak, then I and J are good quantum numbers along with F and m_F. The polarizability coefficients α_0 and α_2 can be related to the absorption oscillator strengths defined earlier. To obtain the appropriate result, it is important to use the fact that the reduced matrix elements of the dipole operator $\hat{p}$ can be written

$$|\langle \gamma_\mu JIF||\hat{p}||\gamma_k J_k I F_k\rangle|^2 = g_F g_{F_k} \begin{Bmatrix} J & I & F \\ F_k & 1 & J_k \end{Bmatrix}^2 \times |\langle \gamma_\mu J||\hat{p}||\gamma_k J_k\rangle|^2, \quad \text{(A16)}$$

where the object defined by the large curly brackets is a 6-j symbol [21]. Then, using this relation, the polarizability coefficients can be expressed in terms of the oscillator strengths Eq. (A11) as follows:

$$\alpha_0 = \frac{e^2 g_J}{m_e} \sum_{k \neq \mu} \frac{\phi_0(F, F_k) f_{\mu k}}{\omega_{k\mu}^2 - \omega^2} g_{F_k} \begin{Bmatrix} J & I & F \\ F_k & 1 & J_k \end{Bmatrix}^2, \quad \text{(A17)}$$

and

$$\alpha_2 = \frac{e^2 g_J}{m_e} \sum_{k \neq \mu} \frac{\phi_2(F, F_k) f_{\mu k}}{\omega_{k\mu}^2 - \omega^2} g_{F_k} \begin{Bmatrix} J & I & F \\ F_k & 1 & J_k \end{Bmatrix}^2, \quad \text{(A18)}$$

where we have ignored the small energy shifts in $\omega_{k\mu}$ that occur due to the hyperfine interaction.

[1] H. Scheffers and J. Stark, Phys. Z. **35**, 1625 (1934); W.D. Hall and J.C. Zorn, Phys. Rev. A **10**, 1141 (1974).

[2] R.A. Alpher and D.R. White, Phys. Fluids **2**, 153 (1959).

[3] Here E denotes electric field; H denotes magnetic field. R. Molof, H.L. Schwartz, T.M. Miller, and B. Bederson, Phys. Rev. A **10**, 1131 (1974).

[4] R.H. Olcutt and R.H. Cole, J. Chem. Phys. **46**, 697 (1967).

[5] T.M. Miller and B. Bederson, Adv. At. Mol. Phys. **13**, 1 (1977).

[6] T.M. Miller and B. Bederson Adv. At. Mol. Phys. **25**, 37 (1989).

[7] M.A. Kadar-Kallen and K.D. Bonin, Phys. Rev. Lett. **68**, 2015 (1992).

[8] P.L. Gould, G.A. Ruff, and D.E. Pritchard, Phys. Rev. Lett. **56**, 827 (1986).

[9] W. Happer and B.S. Mathur, Phys. Rev. **163**, 12 (1967).

[10] B.S. Mathur, H. Tang, and W. Happer, Phys. Rev. **171**, 11 (1968); W. Happer, Prog. Quantum Electron. **1**, 51 (1971).

[11] M.A. Kadar-Kallen, Ph.D. thesis, Princeton University, 1992 (unpublished).

[12] R. Baierlein, *Newtonian Dynamics* (McGraw-Hill, New York, 1983), pp. 140–144.

[13] A more precise description of the properties of the (x, v) phase space is given in Ref. [11].

[14] H. Gould, E. Lipworth, and M.C. Weisskopf, Phys. Rev. **188**, 24 (1969); H. Gould, Phys. Rev. A **14**, 922 (1976).

[15] M.A. Kadar-Kallen and K.D. Bonin, Appl. Phys. Lett. **54**, 2296 (1989).
[16] L.N. Shabanova and A.N. Khlyustalov, Opt. Spektrosk. **56**, 205 (1984) [Opt. Spectrosc. (USSR) **56**, 128 (1984)].
[17] G.V. Marr and D.M. Creek, Proc. R. Soc. London Ser. A **304**, 233 (1968).
[18] V.B. Berestetskii, E.M. Lifshitz, and L.P. Pitaevskii, *Quantum Electrodynamics*, 2nd ed. (Pergamon, Oxford, 1980), pp. 221–246.
[19] L.I. Schiff, *Quantum Mechanics*, 3rd ed. (McGraw-Hill, New York, 1968), p. 155.
[20] A. Dalgarno, Adv. Phys. **11**, 281 (1962).
[21] B.W. Shore, *The Theory of Coherent Atomic Excitation* (Wiley, New York, 1990), pp. 1322–1332.
[22] J. Berkowitz, *Photoabsorption, Photoionization, and Photoelectron Spectroscopy* (Academic, New York, 1979), p. 10.